A&A 641, A52 (2020)
https://doi.org/10.1051/0004-6361/202037792

Astronomy & Astrophysics

Exploring velocity limits in the thermonuclear supernova ejection scenario for hypervelocity stars and the origin of US 708

P. Neunteufel[1,2]

[1] Max Planck Institut für Astrophysik, Karl-Schwarzschild-Straße 1, 85748 Garching bei München, Germany
e-mail: pneun@mpa-garching.mpg.de
[2] University of Leicester, University Road, LE1 7RH Leicester, Leicestershire, UK

Received 21 February 2020 / Accepted 19 June 2020

ABSTRACT

Context. Hypervelocity stars (HVS) are a class of stars moving at velocities that are high enough to make them gravitationally unbound from the Galaxy. In recent years, ejection from a close binary system in which one of the components undergoes a thermonuclear supernova (SN) has emerged as a promising candidate production mechanism for the least massive specimens of this class. The explosion mechanisms leading to thermonuclear supernovae, which include the important Type Ia and related subtypes, remain unclear.

Aims. This study presents a thorough theoretical analysis of candidate progenitor systems of thermonuclear SNe in the single degenerate helium donor scenario in the relevant parameter space leading to the ejection of HVS. The primary goal is to investigate the previously indeterminate characteristics of the velocity spectra for the ejected component, including possible maxima and minima, as well as the constraints arising from stellar evolution and initial masses. Furthermore, this paper addresses the question of whether knowledge of the ejection velocity spectra may aid in the reconstruction of the terminal state of the supernova progenitor, with a focus on the observed object, US 708.

Methods. This study presents the results of 390 binary model sequences computed with the Modules for Experiments in Stellar Astrophysics framework, investigating the evolution of supernova progenitors composed of a helium-rich hot subdwarf and an accreting white dwarf, while avoiding assumption of a specific explosion mechanism as much as possible. The detailed evolution of the donor star as well as gravitational wave radiation and mass transfer-driven orbital evolution were fully taken into account. The results were then correlated with an idealized kinematic analysis of the observed object US 708.

Results. This work shows that the ejection velocity spectra reach a maximum in the range of $0.19\,M_\odot < M_{\rm HVS} < 0.25\,M_\odot$. Depending on the local Galactic potential, all donors below $0.4\,M_\odot$ are expected to become HVSs. The single degenerate helium donor channel is able to account for runaway velocities up to $\sim$1150 km s^{-1} with a Chandrasekhar mass accretor, exceeding 1200 km s^{-1} when super-Chandrasekhar mass detonations are taken into account. Results show that the previously assumed mass of $0.3\,M_\odot$ for US 708, combined with proper motions that have been obtained more recently, favor a sub-Chandrasekhar mass explosion with a terminal WD mass between $1.1\,M_\odot$ and $1.2\,M_\odot$, while a Chandrasekhar mass explosion requires a mass of $>0.34\,M_\odot$ for US 708. This mechanism may be a source of isolated runaway extremely low-mass white dwarfs.

Conclusions. The presence of clear ejection velocity maxima that are terminal accretor mass-dependent, but simultaneously initial-condition independent, provides constraints on the terminal state of a supernova progenitor. Depending on the accuracy of astrometry, it is possible to discern certain types of explosion mechanisms from the inferred ejection velocities alone, with current proper motions allowing for a sub- Chandrasekhar mass SN to explain the origins of US 708. However, more robust reconstructions of the most likely SN progenitor state will require a greater number of observed objects than are currently available.

Key words. binaries: close – supernovae: general – subdwarfs – white dwarfs

1. Introduction

The existence of stars moving at velocities high enough to be unbound from the Galaxy, known as hypervelocity stars (HVS), was first proposed more than three decades ago by Hills (1988). While this initial prediction was followed up by a number of theoretical studies (Hills 1991, 1992), primarily based on the assumption that these objects would result from the interaction of a star or binary star with a massive black hole (MBH, Yu & Tremaine 2003), observational evidence was not forthcoming.

This changed with the discovery of SDSS J090745.0+024507 by Brown et al. (2005). Found in the Sloan Digital Sky Survey data set, this object, also referred to as HVS1, is likely a B-type star with a mass of about $3\,M_\odot$ at a distance of 111 kpc from the Galactic Center and a Galactic rest frame velocity of 696 km s^{-1} (Brown et al. 2007). This object led to a targeted search conducted by Brown et al. (2007), which yielded nine further objects in short order, growing to 23 objects over the following decade (Brown 2015).

Theoretical modeling of the ejection mechanism at this point in time focused heavily on the black hole connection. Bromley et al. (2006) predicted the likely ejection velocity spectrum of HVS produced by the encounter of a binary star with a super massive black hole (SMBH) at the Galactic Center (Sag A^*). O'Leary & Loeb (2008) pointed out that an encounter with a stellar mass black hole in orbit around Sag A^* could also act as a source of HVS with Sesana et al. (2009) coming to the same conclusion regarding intermediate mass black holes (IMBH). The latter mechanism has been suggested as a source of certain B-type HVS (Irrgang et al. 2019). Very recently, the discovery of an A-type star of $2.35\,M_\odot$, moving at a Galactic rest frame velocity of $\sim$1700 km s^{-1}, and which could be traced with high

accuracy back to the Galactic Center (Koposov et al. 2020), has greatly bolstered the viability of the SMBH-encounter scenario. For a review of the state of the art on this ejection mechanism, see Brown (2015).

Alternative ejection mechanisms outside of black hole interaction were initially considered in 2009 when Abadi et al. (2009), based on the spatial distribution of known HVS, proposed multiple body interaction during the passing of a satellite dwarf galaxy through the Milky Way as a possible origin. The proposal by Justham et al. (2009) that some HVS could be former members of close binary system with a white dwarf (WD) companion undergoing a supernova (SN) explosion provided a conceptual bridge to ejection mechanisms that had been previously proposed for runaway stars (RS) that are gravitationally bound to the Galaxy (Blaauw 1961; Hoogerwerf et al. 2001), which had been considered incapable of providing the necessary ejection velocities. This idea was later followed up theoretically for both B and G/K-dwarf type stars in core collapse SNe (Tauris 2015) and hot subdwarfs in the thermonuclear scenario (Neunteufel et al. 2016, 2019).

Observational evidence for the viability of the supernova ejection scenario came when Geier et al. (2015) pointed out that US 708 (HVS2), which was a previously known (Hirsch et al. 2005) helium sdO of N-type, indicating unusually fast rotation, was moving with a greater velocity than originally reported and could not be traced back to the Galactic Center.

More recently, thanks to subsequent observational successes (e.g., Raddi et al. 2019), theoretical interest has focused on the evolution of an SN-ejected HVS in the phase following the supernova explosion (Zhang et al. 2019; Bauer et al. 2019), both based on the assumption of the HVS acting as the former donor star or a partially burnt remnant of the former accretor.

With the advent of the latest generation of large scale astrometric surveys (Gaia Collaboration 2018), a number of new objects (Shen et al. 2018), which had previously been thought to originate from a thermonuclear supernova occurring in a double WD system, as well as a number of additional candidates (de la Fuente Marcos & de la Fuente Marcos 2019), have been discovered. In the same vein, data obtained by the *Gaia* instrument has confirmed the origin of HVS3 (HE 0437−5439) within the Large Magellanic cloud (Edelmann et al. 2005; Irrgang et al. 2018; Erkal et al. 2019). Considering the capabilities of upcoming instruments (e.g., 4MOST: de Jong et al. 2016), further discoveries in this field can be expected.

The supernova ejection scenario for HVS can be considered particularly appealing since, as this paper aims to show, the ejection velocity spectrum for these objects is closely related to the progenitor binary's orbital parameters and mass distribution at the point of HVS ejection. Knowledge of these parameters, which contain information of the state of the exploding companion, can then be used to infer the explosion mechanism of the supernova, which, in the case of thermonuclear events, has not been conclusively resolved to date (see, e.g., review by Hillebrandt & Niemeyer 2000).

Studies of the pre-explosion evolution of close binary systems have been performed in the past (e.g., Ergma & Fedorova 1990; Yoon & Langer 2004a,b; Yungelson 2008; Wang et al. 2013; Neunteufel et al. 2016, 2019), but with a focus not on runaway velocities but on the ignition behavior of the accretor. However, while Han (2008) and Wang & Han (2009) did study the ejection velocity distribution of donor stars ejected from these systems subsequent to a supernova explosion using a population synthesis framework, their parameter space is limited to runaway masses $\geq 0.6\,M_{\odot}$. The present study is meant to remedy this situation in presenting a detailed examination of the parameter space available for close white dwarf binary systems, including initial mass and mass ratio, as well as initial orbital separation, proposed to allow for the occurrence of thermonuclear SNe. As the precise explosion mechanism of these events is currently unresolved, the methodology aims to remain agnostic to this and, therefore, to the precise state of the accretor at the time of creation of the HVS. This paper presents the results of 390 detailed binary evolution models sequences, commenting on the ejection velocity spectra of a variety of proposed explosion mechanisms of thermonuclear SNe, the pre-explosion evolution of the system and the donor star, and the viability of using HVS as probes of thermonuclear SN explosion mechanisms.

It should be emphasized that the focus of this study is HVS ejection by thermonuclear SNe in general, of which Type Ia SNe are considered a subtype, not Type Ia SNe exclusively, whose relatively similar peak luminosity hints at a likewise relatively similar terminal WD mass at the point of explosion (Phillips 1993). However, in the absence of a consensus on the spectral classification of hypothetical progenitor SNe of observed HVS, it is reasonable to assume that WD masses at the point of detonation in these events may be dissimilar to those responsible for Type Ia SNe. This paper can make no statement about the observational properties of the SN event, focusing solely on the velocity of the expected runaway for a certain assumed WD mass.

This report is organized as follows: Sect. 2 presents a brief review of the literature concerning explosion mechanisms of thermonuclear SNe. In Sect. 3, a number of analytical considerations relevant for the investigation of close binary systems are presented. Section 4 describes the numerical tools used in this project and justify the choice of initial model parameters. Section 5 presents the study's findings, commenting on the bulk properties of the sample and observational properties of certain individual cases. Section 6 presents a simple application to the observed object, US 708, using the predictions in the preceding sections. In Sect. 7, the results are discussed, along with a brief summary and conclusions in Sect. 8. A brief investigation of the effects of variations in the initial orbital separation is shown in Appendix A. Section 6 makes extensive use of calculations of the motion of a hypervelocity star in the Galactic potential. As this is slightly beyond the focus of this study, the potential and numerical tools employed here are briefly discussed in Appendix B.

2. Review of applicable explosion mechanisms

While it is widely accepted that thermonuclear SNe result from the thermonuclear detonation of a WD receiving material from a binary companion, the nature of the progenitor system is not well-understood at present. Generally, hypotheses regarding the companion fall into two distinct categories: double degenerate (DD), where the companion in another WD, and single degenerate (SD), where the companion is a non-degenerate star (e.g., a main sequence star)[1]. However, apart from the reasonably well established identity of the exploding object as a WD, uncertainties persist as to its state, especially its mass, at the point of detonation (terminal mass) as well as at the outcome of the explosion. It is classically understood that in systems containing two WDs of sufficient mass, Roche lobe overflow (RLOF) leads to one or both companions being dynamically disrupted before merging,

[1] Note that for our purposes the defining characteristic for categorization into these groups consists solely in the interaction between either two degenerate objects or one degenerate and one non-degenerate object (compare Soker 2013).

with the merged object ultimately detonating (see e.g., Webbink 1984). While it is generally expected that this scenario will leave no bound remnant, certain violent merger scenarios have been predicted to occur on short enough timescales to allow for the ejection of a bound object (Pakmor et al. 2013; Shen et al. 2018).

Note that a dynamical disruption of the mass donor can be avoided in double degenerate systems with relatively small ($q \leq 0.63$) mass ratios (Eggleton 2011). However, as this paper is concerned with the production of non-degenerate HVS, the DD scenario is disregarded for this study. In the SD-scenario, the binary is not expected to merge. Instead, the non-degenerate companion will donate material to the WD (note: this mass transfer, depending on the mass ratio of the system and the evolutionary state of the donor, is not necessarily stable). Based on the prevalent explosion mechanism, which at the time of this writing, is still heavily debated, a thermonuclear explosion is initiated on the WD by one of the mechanisms discussed below as soon as the requisite ignition conditions are reached. If the WD is completely disrupted by the explosion, the donor star is, under the preservation of its orbital angular momentum, flung away from the former location of the binary with a velocity that is slightly greater than its terminal orbital velocity (Bauer et al. 2019). It should be noted that not all hypotheses concerning the mechanism of thermonuclear SNe predict the complete disruption of the WD and, instead, some consider a partially burnt remnant (Vennes et al. 2017).

A number of objects that would fit this scenario have recently been described (Raddi et al. 2019). This would imply that the runaway velocity will be lower than in the case of a complete disruption of the WD (with a possibility of the partially burnt remnant becoming a HVS). While this is doubtlessly important, a closer study of this case is beyond the scope of this paper and is left for future inquiry. As further commented on in Sect. 3, obtainable velocities in the SD supernova ejection mechanism are inversely correlated with the physical radius of the donor star. This circumstance suggests that helium-rich donor stars in their core helium burning phase are the principal candidates for the production of non-degenerate HVS in the supernova ejection scenario. This study, therefore, chiefly considers production mechanisms for thermonuclear SNe which rely on accretion from non-degenerate He-rich donor stars in their core helium burning phase and assumes that the explosion of the WD will leave no appreciable bound remnant.

Keeping this in mind, as well as the importance of the terminal mass of the WD to the runaway velocity, the given test cases fall into three broad categories: Chandrasekhar mass mechanisms, sub-Chandrasekhar mass mechanisms, and super-Chandrasekhar mass mechanisms. The following discussion is conveniently summarized in Fig. 1 and related citations in Table 1, showing likely terminal WD masses as proposed in the literature at the time of this writing.

2.1. Chandrasekhar mass mechanisms

Mechanisms falling into this category are distinguished by the assumption that a thermonuclear SN is initiated when the accreting WD reaches a terminal mass close to the Chandrasekhar mass (Hoyle & Fowler 1960; Arnett 1969; Hansen & Wheeler 1969). While a number of successes in the spectral modeling of explosion mechanisms in this category could be achieved (see e.g., Nomoto et al. 1984; Hillebrandt & Niemeyer 2000), major challenges persist in resolving the dominant one. Prompt detonation at the time terminal mass is attained is generally ruled out (Arnett 1971) on the grounds of a significant overproduction of

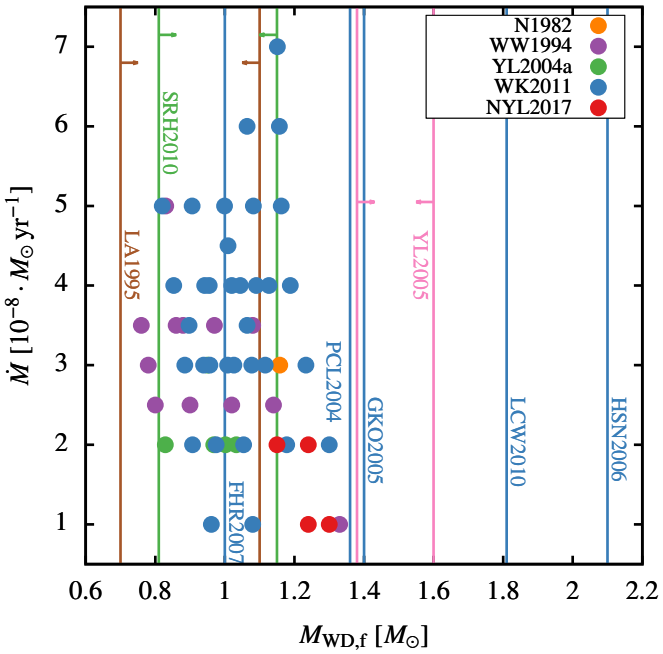

Fig. 1. Representation of the parameters of proposed explosion mechanisms in the parameter space accessible to this study with $\dot{M}$ the mass transfer rate and $M_{\mathrm{WD,f}}$ the proposed total mass of the accreting WD at the point of detonation. If both values are provided by the source, each model is represented as a dot. If the source only provides a single value for $M_{\mathrm{WD,f}}$, the model is represented as a blue line. If a range for $M_{\mathrm{WD,f}}$ is given, it is represented as pairs of colored lines with arrows indicating the position of the corresponding second line. Labels indicate source material as defined in Table 1.

iron group elements (IGE), while pure deflagration models (i.e., including subsonic flame propagation, as opposed to supersonic flame propagation in a detonation) tend to produce insufficient amounts of IGE in addition to featuring insufficiently high ejecta velocities.

A method for overcoming this dichotomy was proposed in the deflagration-detonation scenario (DDT), which presupposes the ignition of core carbon burning in the subsonic regime, transitioning to the supersonic regime during the time the burning front takes to traverse the WD (Khokhlov et al. 1997). While this scenario generally produces isotope yields that are well in agreement with observation, major challenges persist in the self-consistent modeling of the subsonic-supersonic transition, as well as that of the microphysics involved in the propagation of the burning front.

Further uncertainties persist in considering whether the deflagration, once initiated, develops into a detonation after an initial delay (the delayed DDT scenario) – prompt transition into the detonation regime would be akin to the prompt scenario described above – or after a number of "pulses" (the pulsational DDT scenario). These pulses would see one or more increases and subsequent drops in nuclear burning, accompanied by an expansion and contraction of the WD, with CO being converted into IMEs, before the final ignition of a detonation which would then be visible as an SN.

Also included in this category are certain outcomes of systems resulting in a double detonation scenario (this mechanism is more relevant for the sub-Chandrasekhar category and is discussed in greater detail in that context; see Sect. 2.2) as they continue to accrete to within $0.05\,M_\odot$ of the Chandrasekhar mass (Neunteufel et al. 2019), depending on the efficiency of

Table 1. Sources of utilized test cases.

Label	Citation	Method	Additional notes
N1982	Nomoto (1982a,b)	1D SEC	DDet mechanism proposed
WW1994	Woosley & Weaver (1994)	1D SEC	–
LA1995	Livne & Arnett (1995)	2D HS	–
YL2004	Yoon & Langer (2004a)	1D SEC	Included rotational instabilities
PCL2004	Plewa et al. (2004)	2D HS	–
GKO2005	Gamezo et al. (2005)	3D HS	Representative for the $M_{\rm Ch}$-case
YL2005	Yoon & Langer (2005)	1D SEC	Super-$M_{\rm Ch}$-case, differential rotation
HSN2006	Howell et al. (2006)	Observational	Observed Super-$M_{\rm Ch}$, inferred mass
FHR2007	Fink et al. (2007)	3D HS	–
SRH2010	Sim et al. (2010)	1D HS	–
LCW2010	Liu et al. (2010)	1D SEC	–
WK2011	Woosley & Kasen (2011)	1D SEC+HS	–
NYL2017	Neunteufel et al. (2017)	1D SEC	Included rotation+magnetic torques

Notes. Sources for the main test cases used in this study, including the methodology employed by each source: stellar evolution calculation (SEC), hydrodynamical simulation (HS), or observations.

angular momentum transport in the accreting WD. As mechanisms acting at this terminal mass can be considered "classical", observed objects moving with velocities incompatible with terminal masses in the range of $1.35\,M_\odot > M_{\rm d,f} > 1.45\,M_\odot$ will prove to be most interesting.

2.2. Sub-Chandrasekhar mass mechanisms

If thermonuclear SNe can be ignited well below the Chandrasekhar mass, then the initiation of nuclear burning would not be related to the WD's stability against gravitational collapse. The initial "spark" setting off the thermonuclear detonation of the CO core would therefore not be lit at the center of the WD. One mechanism capable of achieving this was first proposed in the 1980s by Nomoto (1980, 1982a). This mechanism, now widely known as the double detonation (DDet) mechanism, posits that a helium layer, accumulated from a helium-rich companion star of some description, on top of the WD's CO core, can act as a detonator for the thermonuclear disruption of the star. Under certain (currently understood relatively well but not completely) circumstances, the ignition of nuclear burning in such a helium layer would lead to a detonation of the helium. The associated detonation shock would then trigger a secondary detonation of the carbon in the WD's core. Terminal accretor masses in this scenario have been argued to be as low as $0.75\,M_\odot$ (Livne & Arnett 1995).

Another mechanism falling into this category, while very similar to the DDet mechanism, is the prompt double detonation (PDDet) or dynamically driven double degenerate double detonation (D6) mechanism. This mechanism relies on turbulent ignition of a thin $<0.05\,M_\odot$ helium layer, accumulated dynamically from a companion (most likely a He-WD or hybrid HeCO WD), setting off a secondary detonation of the accretor's CO core (Pakmor et al. 2013).

2.3. Super-Chandrasekhar mass mechanisms

In the DD scenario, super-Chandrasekhar mass explosions are expected to occur simply if the total mass of the system, containing two sub-Chandrasekhar mass WDs, is sufficiently high. In the SD scenario, however, theory requires super-Chandrasekhar mass detonations to rely on rotation. The effects of rotation on the stability of WDs against gravitational collapse has been of interest to the astrophysical community for some time. Specifically, Yoon & Langer (2005) showed that fully differentially rotating WDs may avoid gravitational collapse at masses up to $2.2\,M_\odot$. Rigid rotation is unable to prevent gravitation collapse at masses higher than $1.5\,M_\odot$ (Hachisu et al. 2012). In either case, an accreting WD, starting at masses sufficiently below the Chandrasekhar mass to allow for the WD to be sufficiently spun up by angular momentum accretion to avoid collapse at the Chandrasekhar mass can be expected to grow beyond it.

After the system detaches, the fast rotation of the WD can then be slowed through mechanisms like tidal interaction, the r-mode instability (see e.g., Yoon & Langer 2004a), or, conceivably, magnetic braking (Mestel 1968). As the rotation of the WD slows (which is expected to occur on timescales of up to Gyr), it becomes progressively less stable against gravitational collapse, which is expected to occur once the WD has lost a certain amount of angular momentum. This scenario, widely known as the spin-up/spin-down (su/sd) mechanism was first proposed some time ago (see e.g., Di Stefano et al. 2011), with significant uncertainties remaining related to explosion physics and the spin-down timescale. However, it is unlikely that a runaway hot subdwarf is produced if the spin-down timescale is very long.

3. Physical considerations

The terminal orbital velocity of a donor star of a given mass $M_{\rm d}$ and radius $R_{\rm d}$ in a binary system undergoing a thermonuclear supernova can be calculated by the widely-used approximation provided by Eggleton (1983):

$$a = \frac{R_{\rm d,RL}}{0.49}\left\{0.6 + \left(\frac{M_{\rm WD}}{M_{\rm d}}\right)^{2/3} \ln\left[1 + \left(\frac{M_{\rm d}}{M_{\rm WD}}\right)^{1/3}\right]\right\}. \quad (1)$$

This includes the assumption that the donor star exactly fills its Roche lobe (i.e., the condition $R_{\rm d} = R_{\rm d,RL}$). The terminal orbital velocity then follows from the Keplerian equation,

$$v_{\rm ej} = \sqrt{\frac{GM_{\rm WD}^2}{(M_{\rm WD} + M_{\rm d})a}}, \quad (2)$$

where $M_{\rm WD} = M_{\rm acc}$ is the mass of the accretor and G is the gravitational constant. If the quantity $R_{\rm d}(M_{\rm d})$ can be expressed analytically, the terminal orbital velocity follows immediately from

Eqs. (1) and (2). However, as $R_d(M_d)$ realistically depends on the structure of the star as well as its current mass-loss rate due to RLOF, a consistent solution of both the stellar structure equations and the orbital evolution of the system is required.

Unlike previous studies (e.g., Brooks et al. 2017; Neunteufel et al. 2019), which included the detailed evolution of the accreting companion, this study treats the accretor as a point mass. This consciously adopted simplification allows for the maintenance of a certain "agnostic" approach towards the explosion mechanism and terminal state of the accretor.

The orbital evolution in binary systems is generally influenced by the effects of magnetic braking (Mestel 1968), tides (Hut 1981), mass transfer, and gravitational wave radiation (GWR, see e.g., Landau & Livshitz 1975). Of these, magnetic braking is thought to be important mainly in solar-type stars and neglected in He rich stars like the ones under consideration here, as the systems considered here can be thought of as circularized and tidally locked subsequent to the most recent common envelope (CE) phase; with "most recent" referring to the CE phase immediately preceding the formation of the He donor. Tides, as well as the possibility of non-conservative mass transfer, are neglected.

The orbital evolution of these systems are, therefore, dominated by mass transfer and GWR. While angular momentum loss due to GWR acts to decrease orbital separation under all circumstances, the angular momentum transported during mass transfer may act to either increase or decrease orbital separation depending on the system's mass ratio, with $q = M_d/M_{acc} < 1$ associated with increasing orbital separation and vice versa. In the systems under consideration, RLOF is induced either through an increase of the donor star radius or decrease of the orbital separation due to GWR. Once the system evolves into a semidetached state, further evolution of the orbit is driven by both GWR and angular momentum transfer.

Eggleton (2011) gives, for GWR and neglecting mass transfer,

$$\frac{\dot{a}}{a} = -\frac{2}{\tau_{GR}}, \tag{3}$$

with a the semi-major axis and the gravitational merger timescale,

$$\tau_{GR} = \frac{5}{32}\frac{c^5 a^4}{G^3(M_1+M_2)M_1M_2}, \tag{4}$$

and for mass transfer, neglecting GWR,

$$\frac{\dot{a}}{a} = 2\frac{\dot{M}_1}{M_1+M_2}\frac{q^2-1}{q}. \tag{5}$$

Note that Eq. (5) implies that the evolution of the orbital separation is independent of the mass transfer rate if $q = 1$. Comparing Eqs. (4) and (5) yields, with the assumption $q < 1$ and the demand that $\dot{a}/a > 0$ the condition,

$$\dot{M}_1 < \dot{M}_{crit} = -\frac{32}{5}\frac{G^3}{c^5 a^4}\frac{(M_1+M_2)M_1^2M_2^2}{M_1-M_2}, \tag{6}$$

as derived by Tutukov & Yungelson (1979). Due to its inverse proportionality to the fourth power of a, Eq. (6) is usually fulfilled by default in most systems containing an ordinary star, whose physical radius is on the order of one magnitude greater than that of a hydrogen-depleted star of comparable mass. With gravitational merger timescales being comparable to the mass transfer timescales ($\tau_{MT} = \frac{\dot{M}_1}{M_1+M_2}$) in the systems under consideration here, the sign of the time derivative of the orbital separation is to be determined by Eq. (6).

4. Numerical methods and initial model parameters

The fundamental methodology of this study consists of the detailed calculation of the orbital evolution of close He-star+WD binaries. This is accomplished using the Modules for Experiments in Stellar Astrophysics (MESA) framework (Paxton et al. 2011, 2013, 2015, 2018) in its release 11398.

The stellar and binary evolution code MESA is publicly available and well established, capable of treating the evolution of single stars as well as that of the orbital parameters of binary systems. It offers a variety of prescriptions to calculate mass loss due to RLOF. For systems of this type, the mass loss prescription provided by Ritter (1988), implemented as MESA-option `mdot_scheme = "Ritter"`, is considered most appropriate. This scheme relies on implicitly solving

$$R_{d,RL} - R + H_P \cdot \ln\left(\frac{\dot{M}}{\dot{M}_0}\right) = 0, \tag{7}$$

where H_P is the photospheric pressure scale height, R the stellar radius as defined by the photosphere, and $R_{d,RL}$ the Roche lobe radius, with R_{RL} calculated according to Eq. (1).

This study is mostly concerned with the ejection velocity of donor stars ejected from systems with terminal accretor masses in the range $1.1\,M_\odot \leq M_{t,acc} \leq 1.5\,M_\odot$. In order to provide sufficient coverage of the grid, initial accretor masses were chosen in the range of $0.5\,M_\odot \leq M_{t,acc} \leq 1.2\,M_\odot$ in steps of $0.05\,M_\odot$. Initial donor star models range in mass between $0.4\,M_\odot$ and $1.0\,M_\odot$ with solar metalicity. As per Eq. (1), large stellar radii lead to lower ejection velocities. Limiting this study to likely production mechanisms of hypervelocity stars originating in the Galactic disk, this condition excludes post-HeMS stars due to the requirement to exceed the Galactic escape velocity during ejection. Calculations are therefore terminated if the donor stars reaches the end of its core helium burning phase before the onset of RLOF.

4.1. Initial models

The initial states of the employed donor models are summarized in Fig. 2. These initial models are created by initializing a hydrogen-depleted pre-MS model using the MESA-supplied option `create_pre_main_sequence_model = .true.`, allowing it to settle on the HeMS, relaxing it further for a thermal timescale (He-rich models like this tend to contract by 1–5% after reaching the HeMS). The donor model is then placed in a binary system with appropriate characteristics. Initial orbital separations $a_{init}(\xi)$ were chosen such that Eq. (1) satisfies $R_{d,RL} = \xi \cdot R_d$ with ξ an arbitrary dimensionless parameter. Depending on the individual component masses within the given ranges, a system of the present configuration is not expected to interact during the donor's HeMS lifetime at all for orbital radii $a_{init}(\xi > 1.01)$. The most viable choice is deemed to be $a_{init}(\xi = 1.005)$ with a secondary sample of $a_{init}(\xi = 1.01)$ (see Appendix A). This increase only results in a comparably small increase in the initial period of the system. However, as shown in Neunteufel et al. (2019), donor stars of an initial mass $\gtrsim 0.8\,M_\odot$ tend to reach the end of core helium burning disproportionally quickly while those of lower mass $\lesssim 0.5\,M_\odot$ tend to evolve slowly enough to not have experienced significant increase in mass or metalicity before reaching GWR-induced RLOF. While this approach somewhat limits predictive power in intermediate masses, upper and lower limits should be adequately addressed. Initial periods resulting from this prescription are shown in Fig. 2C.

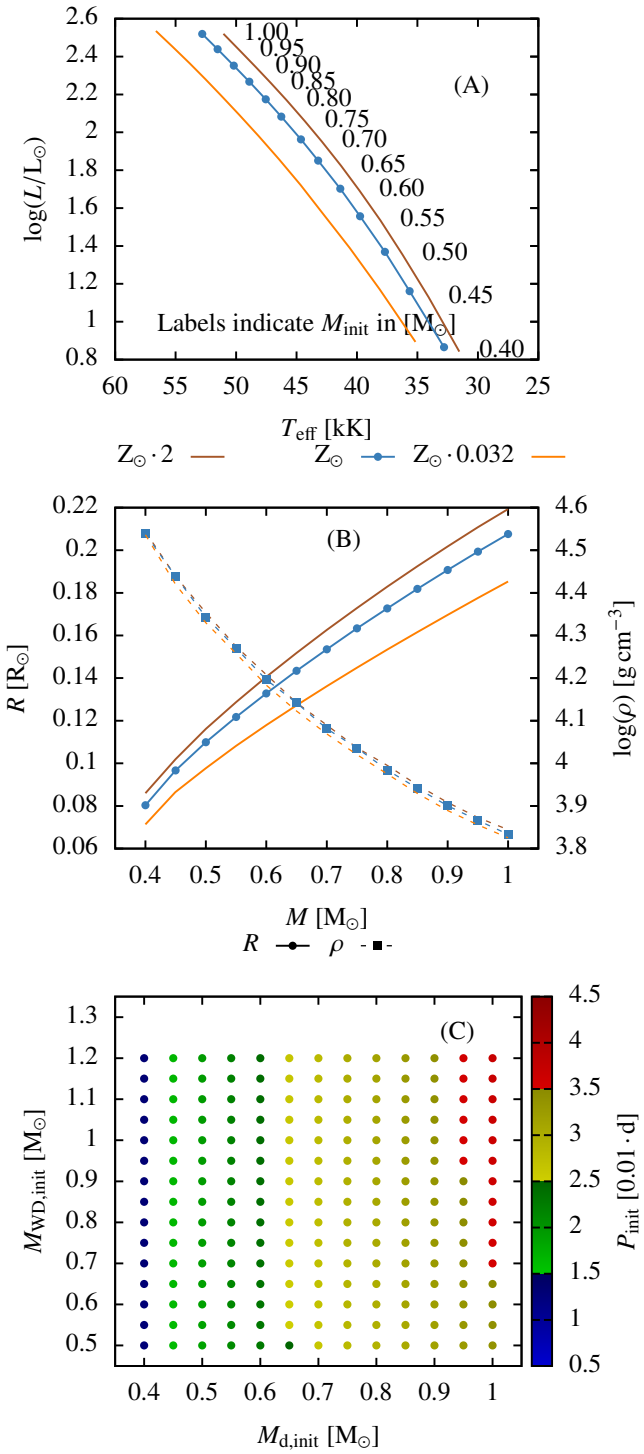

Fig. 2. Relevant initial parameters of the utilized He-donor star models. *Panel A*: position of each model in the HR-diagram, with labels corresponding to initial mass in units of $M_\odot$. Colors indicate initial metallicity in units of the solar metalicity $Z_\odot$ with the solar metalicity used in this study. *Panel B*: initial radius $R_{\rm init}$ in units of the solar radius $R_\odot$ and central density $\rho_{\rm c}$ with colors corresponding to metalicity as in panel A. *Panel C*: initial periods, according to the constraints discussed in Sect. 4.1 with respect to the initial masses of both components.

4.2. Stopping conditions

Computations are terminated either when the donor star's core helium abundance decreases below $Y_{\rm core} = 10^{-3}$ or if the donor star's mass drops below $0.18\,M_\odot$. The first condition is motivated by the desire to focus on the production of hypervelocity hot subdwarfs. Furthermore, the coincident expansion of their envelopes will result in increased mass transfer rates and, therefore, according to Eq. (6), an increase in orbital separation and, consequently, decreased ejection velocities. While further investigation of these hypothetical post-hot-subdwarf runaways is of some interest, it is beyond the scope of this paper. The second condition is warranted due to the limitations of the equation of state (EOS) as currently implemented in MESA as donor star models in their proto-WD phase (i.e., $M < 0.3\,M_\odot$) tend to cross into regions of the parameter space with insufficient coverage (see Paxton et al. 2019, Appendix A), resulting in numerical artifacts or unresolvable models. Specifically, these instabilities occur as sufficient amounts of unburnt helium from the outer layers of the star are removed, exposing the formerly burning and metal-enriched core layers, which at this point, would be cool and sparse enough lie outside the coverage of the EOS. It is found that this problem is largely avoided by halting the simulation at $0.18\,M_\odot$, as most models with both more massive and significantly metal-enriched cores will have left the HeMS (and, consequently, have been removed by the first stopping condition) at this point with remaining models possessing either less massive or sufficiently pristine cores.

5. Ejection velocity spectra

The principal aim of this study is to provide ejection velocity spectra for hypervelocity runaways produced in the He-star+WD channel for thermonuclear SNe. An ejection velocity spectrum, for the purposes of this paper, is composed of the expected ejection velocities of a runaway, depending on the terminal mass of the runaway, for a single terminal WD mass. In order to remain unbiased towards the plethora of proposed explosion mechanisms, as discussed in Sect. 2, which would impose systematic constraints on the derived ejection velocity spectra, a range of terminal WD masses are taken into consideration.

5.1. Partial spectra

Contribution of individual binary model sequences to the ejection velocity spectra for any particular terminal WD mass ($M_{\rm WD,f}$) are shown in Fig. 3. The entire spectrum for any particular choice of $M_{\rm WD,f}$, as derived in this study is then composed of all binary system states with the same value of $M_{\rm WD,f}$. This means that rather than being determined by the evolution of the orbital velocity of an individual binary model sequence, the ejection velocity spectrum is composed of that belonging to the systems in the $v_{\rm orb}$–$M_{\rm d}$ parameter space, where the mass of the accretor is equal to the requested value of $M_{\rm WD,f}$ across multiple model sequences. In the partial spectra seen in Fig. 3, a clear correlation between orbital velocities and the terminal mass of the accretor, independent of both initial masses is apparent. Individual tracks exhibit a maximum of the orbital velocity, located in the range of $0.2\,M_\odot < M_{\rm d} < 0.25\,M_\odot$. As the full ejection velocity spectra are essentially determined by the shapes of numerous individual tracks, this feature is also expected in the complete spectra.

5.2. The ejection velocity maximum

As previously argued, the maximum in ejection velocities exhibited by individual model sequences is expected to translate to the full spectra. This indicates that for each assumed value of $M_{\rm WD,f}$,

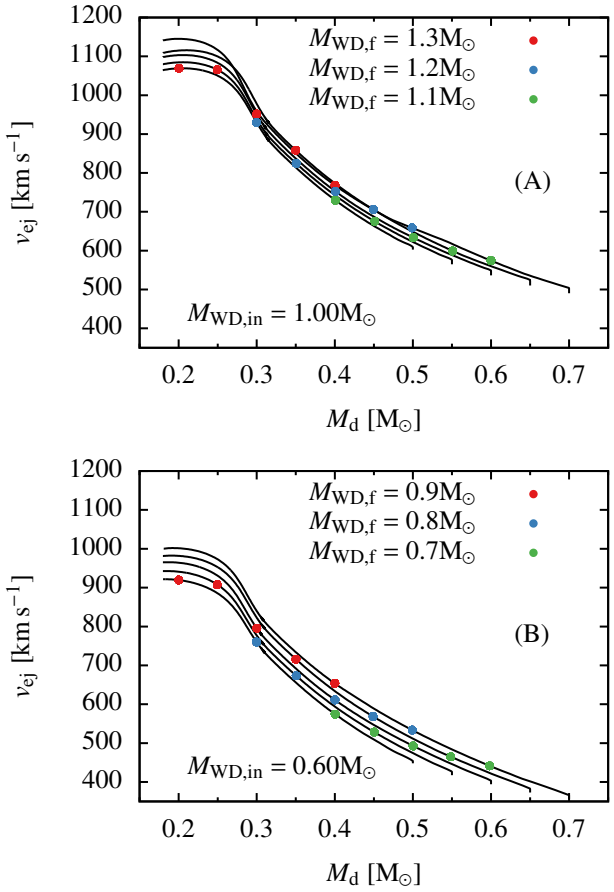

Fig. 3. Representative model sequences detailing the evolution of individual systems in the M_d–v_{ej} space. $M_{WD,in}$ is the initial accretor mass for each of the model sequences with $M_{WD,in} = 1.00\,M_\odot$ in *panel A* and $M_{WD,in} = 0.60\,M_\odot$ in *panel B*. Each dot represents a single model with terminal accretor mass $M_{WD,f}$. Velocities given with respect to the center of mass of the progenitor binary.

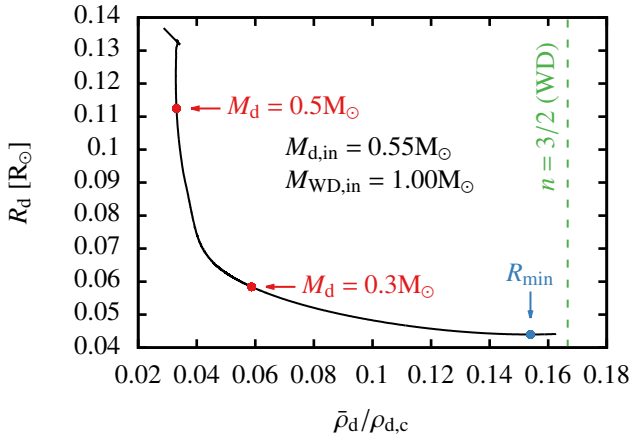

Fig. 4. Radius of the donor star (R_d) in relation to the quotient ($\bar{\rho}_d/\rho_{d,c}$) for the same system as in Fig. 5. The minimum radius R_{min} is reached at a mass of 0.20 $M_\odot$ in this model sequence.

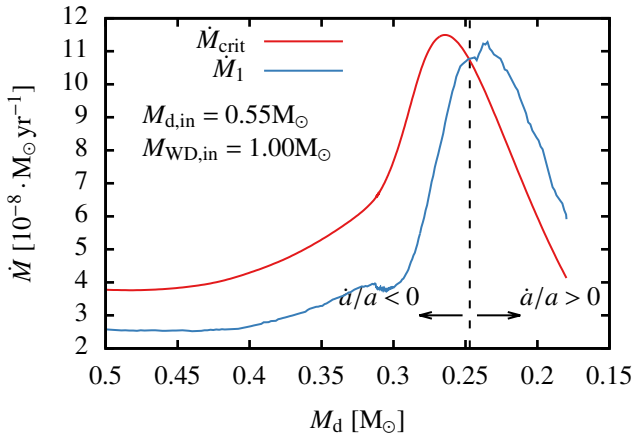

Fig. 5. Comparison between the critical mass transfer rate $\dot{M}_{crit}$ for increasing a as defined in Eq. (6) and the actual mass transfer rate $\dot{M}_1$ for a representative system with respect to donor mass M_d. Initial masses $M_{d,in}$ and $M_{WD,in}$ are as indicated.

there is a maximum ejection velocity $v_{ej,max}(M_{WD,f})$. Consequently, any observed hypervelocity runaway with an inferred ejection velocity higher than $v_{ej,max}(M_{WD,f})$ for an assumed $M_{WD,f}$ must necessarily have been ejected either from a system with a higher $M_{WD,f}$ or by a different mechanism altogether. Any such observation is especially auspicious in the case of $M_{WD,f} \sim 1.4\,M_\odot$. The occurrence of this maximum is driven by the widening of the binary as the donor star becomes more degenerate once its mass drops below the value needed for sustained helium burning. This is the 0.3 $M_\odot$-limit mentioned above. As the donor star loses sufficient mass to drop below this limit, the lack of energy generation by nuclear fusion leads to contraction on the thermal timescale concurrent with a reconfiguration of the star's structure to become more degenerate. This reconfiguration is conveniently illustrated by the evolution of the quotient $\bar{\rho}_d/\rho_{d,c}$ (i.e,. the donor star's average density divided by its central density). This quotient is a well known quantity in polytropic stellar models with

$$\frac{\bar{\rho}}{\rho_c} = \left(-\frac{3}{z}\frac{\mathrm{d}w}{\mathrm{d}z}\right)_{z=z_n}, \tag{8}$$

where z_n are the solutions to the Lane-Emden equation,

$$\frac{1}{z^2}\frac{d}{\mathrm{d}z}\left(z^2\frac{\mathrm{d}w}{\mathrm{d}z}\right) + w^n = 0, \tag{9}$$

and n the polytropic index. Low-mass WDs are well approximated by polytropic equations of state with $n = 3/2$ (see e.g., Kippenhahn et al. 2012). In the systems discussed here, as the donor star loses mass, the quotient $\bar{\rho}_d/\rho_{d,c}$ is thus expected to evolve towards values compatible with a polytropic index of $n = 3/2$. An example of this is shown in Fig. 4. It is noteworthy to observe that as the donor star approaches $(\bar{\rho}_d/\rho_{d,c})_{z_n=z_{3/2}}$, its radius passes a minimum. This inverse correlation (compared to main sequence stars) of mass and radius is a well known property of WDs. As the donor star approaches a radius minimum, the mass transfer rate, as shown in Fig. 5, increases. As shown, this increase in mass transfer is sufficient to exceed the critical mass transfer rate defined in Eq. (6), in turn leading to an increase of the orbital separation and, hence, a decrease of the orbital and ejection velocity.

In the present sample, the radius minimum is generally attained in the range $0.19\,M_\odot < M_d < 0.25\,M_\odot$ (Fig. 6). Objects in this range, as indicated in Fig. 4, would be characterized as proto-WDs which, following a period on further contraction, would form a population of low-mass, high velocity runaway WDs. However, as these objects are likely to only properly settle on the WD cooling sequence a considerable time after ejection and, corresponding to their high ejection velocity, a significant

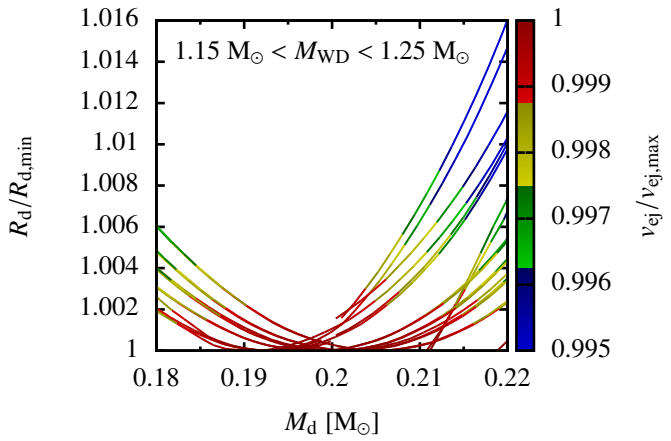

Fig. 6. Mass-radius relationship of donor stars in the vicinity of the ejection velocity maximum. The mass-dependent donor star radius (R_d) is normalized to the minimum radius of that particular model sequence ($R_{d,min}$), the mass dependent ejection velocity, indicated by the color bar, (v_{ej}) is analogously normalized to the maximum ejection velocity of the same model sequence. For clarity, only tracks in the vicinity of an accretor mass in the range 1.15 $M_\odot$ < M_{WD} < 1.25 $M_\odot$ are shown.

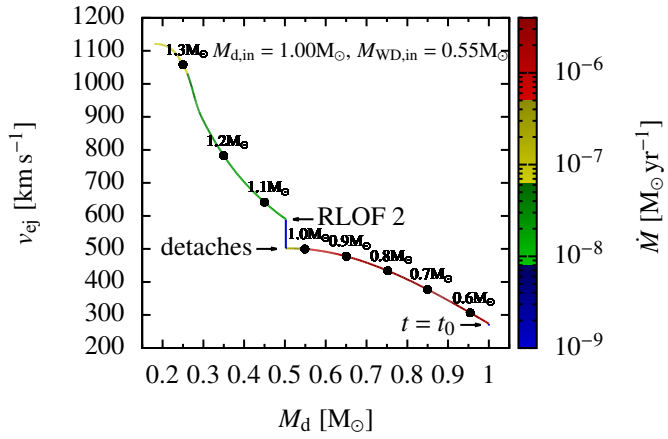

Fig. 7. Model sequence in M_d–v-space of a single binary system with initial masses $M_{d,in}$ and $M_{WD,in}$, i.e., $q > 1$. Color indicates the current mass transfer rate $\dot{M}$. Labels along the graph indicate the current accretor mass. $t = t_0$ is indicated as well as the points where the system detaches and undergoes a second RLOF. Velocity given with respect to the center of mass of the progenitor binary.

distance from their point of origin, observation of such an object as a high velocity extremely low-mass (ELM) WD is deemed unlikely, though not impossible. This scenario is similar to the one proposed by Justham et al. (2009) but has to be tempered with the notion of a large fraction if not all of the currently observed ELM WDs being part of a binary (Brown et al. 2020).

5.3. Bifurcations

The orbital velocity evolution of a system with initial mass ratio $q > 1$ is shown in Fig. 7. As can be seen, the system undergoes two distinct phases of mass transfer: A "fast" phase of high mass transfer rates, followed by a "slow" phase of low mass transfer rates. In stars that only undergo core burning, the mass transfer timescale is generally comparable to the donor star's nuclear timescale (i.e., $\tau_{nuc} \sim \tau_{RLOF}$), however, in systems with $q > 1$, angular momentum transfer due to RLOF additionally acts to decrease the system's orbital separation, leading to enhanced mass transfer. However, as the donor star is initially the more massive companion in these systems, it is expected to initially orbit with a lower orbital velocity. The donor star will lose mass to the accretor until $q = 1$ is reached, at which point angular momentum transfer will act to increase the orbital separation (see Eq. (5)) until the system detaches. Prior to the point of detachment, the orbital velocity of the donor star is generally be lower than in systems with $q < 1$ at the same donor star mass. Subsequent to detachment, the components then evolve in isolation until angular momentum loss due to GWR has decreased the orbital separation sufficiently to initiate a second RLOF. The lower orbital velocities prior to detachment lead to the presence of a secondary branch in the full ejection velocity spectra. However, due to the limited nature of the initial parameter space in this study, this secondary branch is only resolved in the spectra corresponding to the lowest terminal WD masses.

5.4. Complete spectra

Full ejection velocity spectra in the range 1.0 $M_\odot$ < $M_{WD,f}$ < 1.5 $M_\odot$ are shown in Fig. 8. Note, as may naively be expected, that the maximum ejection velocity is correlated with $M_{WD,f}$ and the presence of an ejection velocity maximum in the range of 0.19 $M_\odot$ < M_d < 0.25 $M_\odot$ for all values of $M_{WD,f}$. In panel A with $M_{WD,f} = 1.0\,M_\odot$, a bifurcation of the ejection velocity spectrum, as described above, is visible. It should further be noted that with increasing values of $M_{WD,f}$, the maximum donor star mass shown in each panel decreases. This is only partially a consequence of the choice of initial parameter space, as systems that do not interact during the helium main sequence of the donor star are excluded from this plot. Donor stars of high initial mass tend to evolve quickly enough to avoid RLOF during the helium main sequence at the initial orbital separations chosen in this study and are therefore removed from the sample. For these systems to produce an SN during the core helium burning stage, the donor would have to full its Roche lobe entirely directly subsequent to the most recent CE phase.

Systems in the entire considered range of $M_{WD,f}$ are capable of producing hypervelocity stars, assuming ejection occurs in the Solar neighborhood; higher mass runaways ($\gtrsim$0.5 $M_\odot$) are less likely to become unbound from the Galaxy depending on both the terminal WD mass, the local Galactic escape velocity, and ejection direction. As such, the local Galactic escape velocity should be compared with the ejected companion's space velocity immediately following the SN event. Further, as seen in Fig. 8E, local Chandrasekhar mass explosions can be expected to always produce a hypervelocity hot subdwarf. Ejection velocities higher than 1000 km s^{-1} can be expected for terminal WD masses $\gtrsim$1.1 $M_\odot$. The spread in the ejection velocity spectra (i.e., the presence of multiple ejection velocities for a single value of M_d) is a consequence of the degeneracy of multiple initial systems for a set of terminal WD masses and terminal donor masses. The spread is then a consequence of each donor star in the degenerate set having lost a different amount of mass to the accretor during a mass transfer episode of different length, leading to a slightly different structure and chemical composition in each case. However, the spread is small enough that the dependence of the ejection velocity on the runaway mass is still clearly indicated. The inferred ejection velocity of the runaway hot subdwarf US 708 according to Geier et al. (2015) is 998 km s^{-1}. This ejection velocity can be reached by any explosion involving an accretor mass $M_{WD,f} = 1.1\,M_\odot$. However, importantly, only if $M_{d,f} > 0.3\,M_\odot$ in systems with $M_{WD,f} \geq 1.4\,M_\odot$.

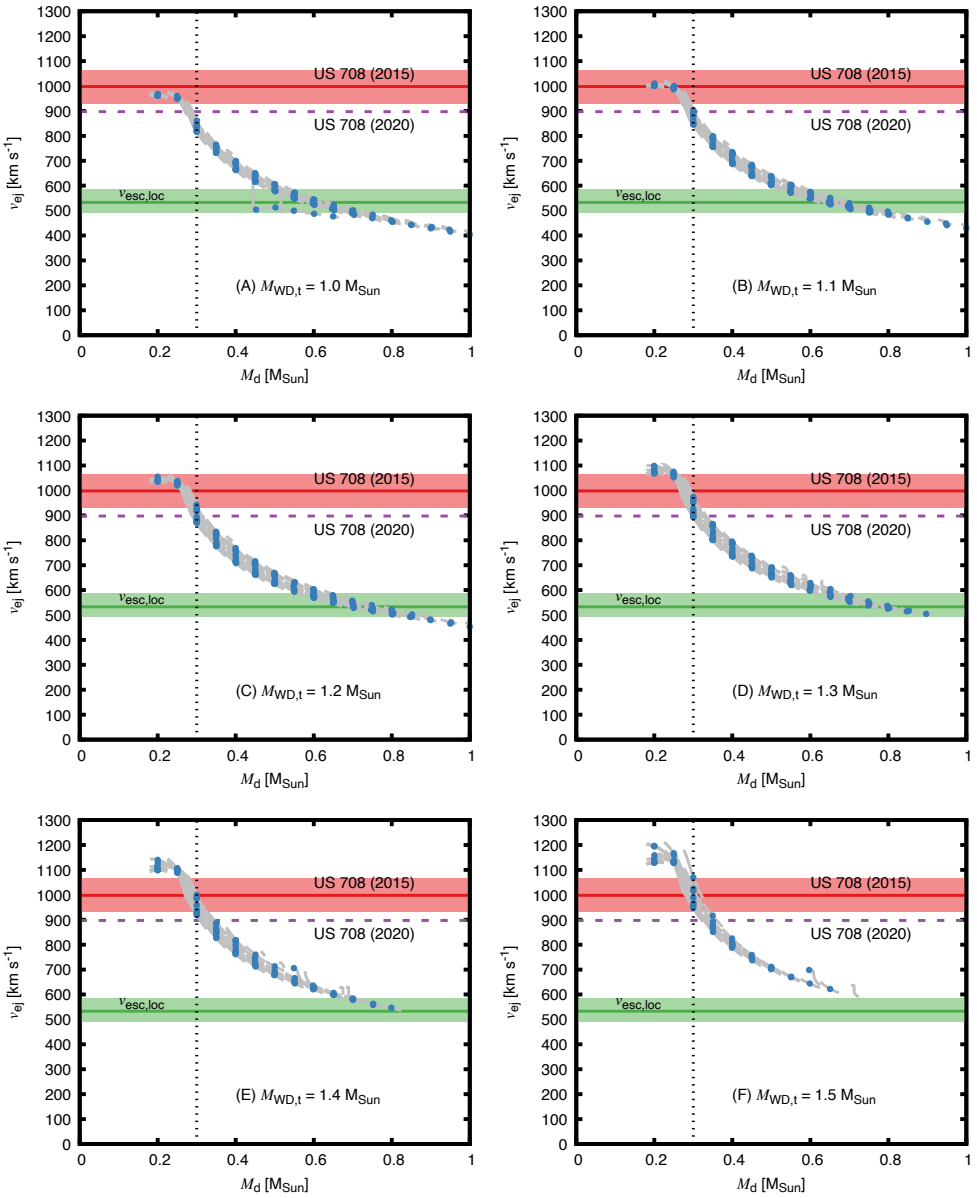

Fig. 8. Ejection velocity spectra for indicated terminal accretor masses ($M_{WD,t}$). M_d and v_{ej} are the terminal mass and expected ejection velocity with respect to the center of mass of the progenitor binary of the remnant runaway hot subdwarf. The blue dots indicate the exact state of the system when the accretor reaches the indicated $M_{WD,t}$. Lines indicate the evolution of the system in an envelope from $M_{WD,t} - 0.025 \cdot M_\odot < M_{WD,t} < M_{WD,t} + 0.025 \cdot M_\odot$. The dotted purple line indicates $M_{rem} = 0.3\,M_\odot$, below which core helium burning ceases. The inferred ejection velocity of US 708 according to Geier et al. (2015) and current proper motions provided by *Gaia* DR2 (Gaia Collaboration 2018), represented by the solid red and dashed purple lines respectively, and local Galactic escape velocity according to Pifl et al. (2014), including error bars, are given for orientation.

With an inferred ejection velocity calculated from the proper motions provided in *Gaia* DR2, (Gaia Collaboration 2018) of 897 km s^{-1}, the terminal accretor mass could be as low as $M_{WD,f} = 0.85\,M_\odot$. In this case, the minimum terminal accretor mass for $M_{d,f} > 0.3\,M_\odot$ is, notably, $M_{WD,f} = 1.1\,M_\odot$. The case of US 708 will be discussed in greater detail in Sect. 6.

As seen in Fig. 8F, $1.5\,M_\odot$ explosions are capable of propelling a runaway to velocities up to 1200 km s^{-1}, which is about 100 km s^{-1} slower than the D6-2 object as found by Shen et al. (2018). However, it should be mentioned that the reliability of this particular measurement is being debated in literature (Scholz 2018).

5.5. Runaway velocities as a probe of the pre-explosion progenitor state

As seen in Sect. 5.4, given a constant value, $M_{WD,f}$, ejection velocities are a strong function of $M_{d,f}$. Figure 9 shows the maximum ejection velocities obtained in this sample with respect to the terminal WD mass (both the total maximum and the maxima for a given minimum mass of the runaway). As the depicted values are the theoretical maxima of ejection velocities, they can be used to obtain constraints on the parameters of the progenitor binary at the time of explosion. Specifically, since higher ejection velocities require higher terminal WD masses, but higher terminal donor star masses inhibit them, knowledge of the ejection velocity provides constraints on the parameter space of both the donor and the accretor mass. US 708 is given as an example in this plot, with a terminal WD mass in the range of $1.07\,M_\odot < M_{WD,f} < 1.39\,M_\odot$, with corresponding values of $0.18\,M_\odot < M_{WD,f} < 0.31\,M_\odot$ for the terminal donor star mass based on proper motions obtained by Geier et al. (2015). Based on proper motions obtained from *Gaia* DR2 (Gaia Collaboration 2018), these values are amended to $0.85\,M_\odot < M_{WD,f} < 1.39\,M_\odot$, with corresponding values of $0.18\,M_\odot < M_{WD,f} < 0.35\,M_\odot$. In both cases, this study assumes sub-Chandrasekhar or Chandrasekhar-mass explosions. Also note that, as calculated by Bauer et al. (2019), the terminal donor mass may be as much as twice that of the current mass of the eventually observed runaway.

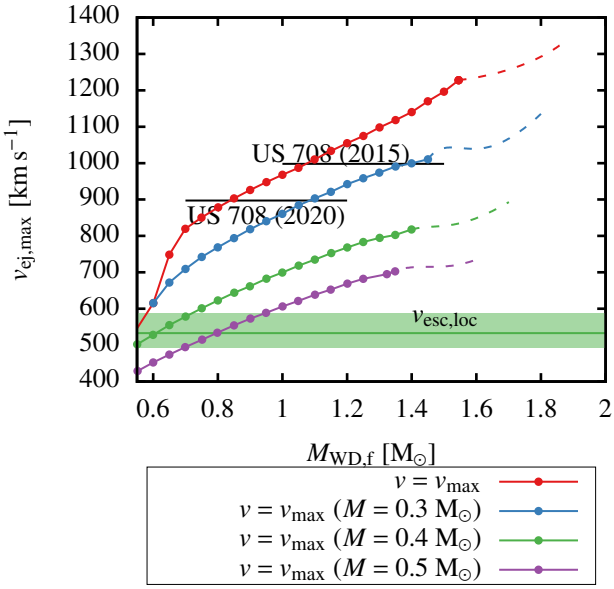

Fig. 9. Maxima of all ejection velocity spectra as given in Fig. 8 with respect to terminal accretor mass ($M_{WD,f}$), where v_{max} indicates the absolute maximum and $v_{max}(M_d)$ the maximum, with respect to the center of mass of the progenitor binary, for a given mass of the ejected companion (M_d). Black lines indicate inferred ejection velocities as calculated by Geier et al. (2015) and using proper motions as provided by *Gaia* DR2 (Gaia Collaboration 2018). The dashed lines indicate the expected continuation of the maxima towards areas of the parameter space insufficiently covered by the grid.

5.6. Rotation

While the question of the rotational velocity of the ejected HVS is not the primary subject of this study, the fact of its potential accessibility to observation merits a brief discussion. The terminal surface rotational velocities of the ejected component are shown in Fig. 10. Excepting bifurcations, as discussed in Sect. 5.3, rotational velocities are expected to be uniformly higher than $v_{f,rot} = 270\,\mathrm{km\,s^{-1}}$ and lower than $v_{f,rot} = 326\,\mathrm{km\,s^{-1}}$, independent of the terminal accretor mass. With respect to the critical rotational velocity $v_{rot,crit}$, this corresponds to a range between $0.29 \cdot v_{rot,crit}$ and $0.33 \cdot v_{rot,crit}$. The reason for the uniformity of rotational velocities lies in the underlying assumption of tidal locking, as donors of equal mass but increasing accretor masses will find themselves in correspondingly wider systems. This uniformity was also noted by Geier et al. (2015), with the upper limit presented in this study in reasonably good agreement with the inferred, model-dependent, initial rotational velocity of $v_{f,rot} =\sim 350\,\mathrm{km\,s^{-1}}$, as derived by Geier et al. (2015). The assumption of tidal locking necessarily leads to a direct correlation of rotational and ejection velocity. The differing rotational velocity predicted at the lower limit (just as the spread seen in the ejection velocity spectra) indicates that the donor star's structure and evolutionary history does have a noticeable effect on the final state of the system. Remarkably, the spread of rotational velocities is comparable to that of ejection velocities, as shown in Fig. 8. As can further be seen, the predicted terminal rotational velocities are larger by at least a factor of 2.3 than the observed current $v_{rot} \sin i = 115 \pm 8\,\mathrm{km\,s^{-1}}$ of US 708. Here it should be borne in mind that the radius of the ejected donor star is unlikely to correspond to the rotational velocity post-ejection. This was also noted by Geier et al. (2015). The decrease in velocity can be explained by the star's post-ejection evolution on the extreme horizontal branch under conservation of angular momentum without the invocation of an SN interaction. However, it should also be emphasized that the post-ejection evolution is likely strongly dependent on the question of ongoing nuclear processes inside the star, with stars below the threshold for helium burning reacting differently than stars above this threshold. Therefore, the thermal response to ejecta impact may still be important, as indicated by the results presented by Bauer et al. (2019).

6. The case of US 708

As mentioned in Sect. 1, the hypervelocity runaway US 708 (HV2, SDSS J093320.86+441705.4, *Gaia* DR2 815106177700 219392) is classified as a helium-rich hot subdwarf. Stars of this type are found at the blue end of the horizontal branch and are thought, most significantly for the purposes of this study (although not exclusively), to products of close binary evolution. An extensive discussion of the properties of these objects is beyond the scope of this paper. For a thorough review, see Heber (2009, 2016).

In Geier et al. (2015), a current mass of 0.3 $M_\odot$ for US 708 was adopted (due to the unavailability of a reliable mass measurement), yielding a likely terminal WD mass of 1.3 $M_\odot$. With the predictions presented in Sect. 5, this assumption can be checked for consistency. This is done via the following prescription:

1. The current mass of US 708 is allowed to serve as a free parameter. As distance was determined spectroscopically by Geier et al. (2015), this would impact the determination of the current space velocity, which would then rely solely on proper motion and radial velocity.
2. Using kinematic analysis (see Appendix B) and assuming ejection in the Galactic disc, a mass-dependent inferred ejection velocity is obtained, taking into account the local Galactic rotation.
3. The resulting ejection velocities are compared with the ejection velocity spectrum for a given terminal WD mass.

Regarding the second point, it should be mentioned that assuming ejection in the Galactic disc is not necessarily warranted, as the star may originate outside the disc, for example, in a globular cluster, correspondingly affecting inferred ejection velocities. Assuming similar structure, the mass (M) and luminosity (L) of two stars are approximately correlated through the homology relation (see e.g., Kippenhahn et al. 2012):

$$\frac{L_1}{L_2} = \left(\frac{M_1}{M_2}\right)^3 \left(\frac{\mu_1}{\mu_2}\right)^4, \tag{10}$$

with μ the mean atomic weight, which is assumed to remain unchanged in this instance. Using the luminosity as calculated in Eq. (10), the distance can then be adjusted by assuming a constant apparent magnitude.

As observational characterization of US 708 has advanced somewhat since 2015, with new proper motion data published in the *Gaia* data release 2 (Gaia Collaboration 2018), but reliable parallax distances and updated radial velocities still unavailable, the following kinematic analysis is performed using two distinct sets of proper motion parameters. The first set relies on the data obtained by ground-based observations published in Geier et al. (2015) (labeled "2015" throughout the paper) and the other on the more recent values obtained by the *Gaia* instrument and published in Gaia Collaboration (2018) (labeled "2020" throughout the paper). Numerical values are given in Table 2.

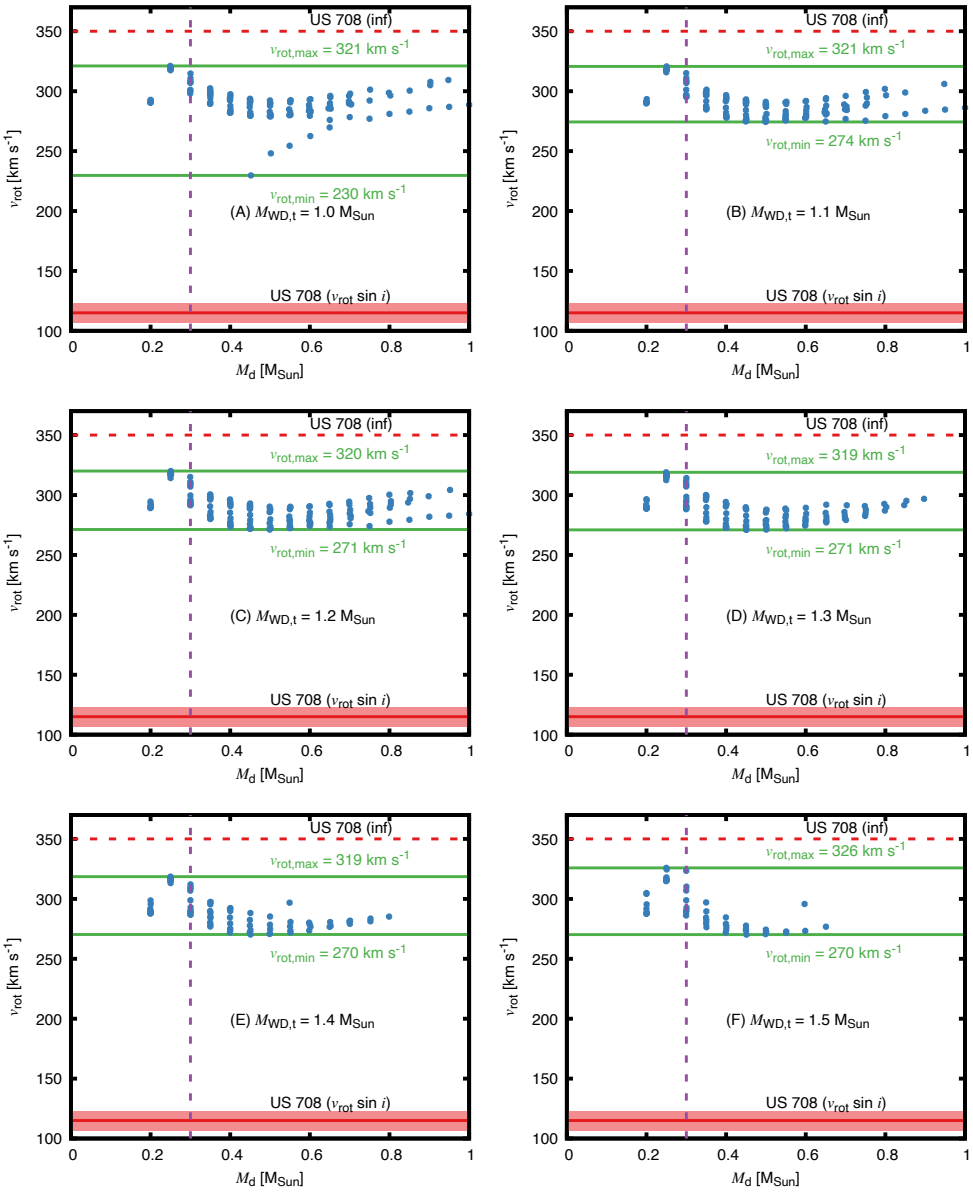

Fig. 10. Same as Fig. 8, but showing the ejected companion's surface rotational velocity at the time of ejection with the observed current $v_{rot} \sin i$, including error bars, given for comparison, with the red dashed line indicates the inferred surface rotational velocity at ejection according to Geier et al. (2015). Green lines indicate the minimum and maximum velocity found in the sample, as labeled.

Table 2. Proper motions utilized in kinematic analysis.

Data set	$\mu_\alpha \cos(\delta)$ [mas yr^{-1}]	μ_δ [mas yr^{-1}]
2015	-8.0 ± 1.8	9.1 ± 1.6
2020	-5.363 ± 0.391	1.285 ± 0.382

In the absence of accessible newer data, the values of visual magnitude ($m_g = 18.668 \pm 0.008$ mag) and heliocentric radial velocity ($v_{helio} = 917 \pm 7$ km s^{-1}) are adopted unchanged from Geier et al. (2015). As the determination of proper motion and radial velocity does not rely on an adopted mass or luminosity, they are kept constant in the calculation of the mass-dependent space velocity. The reader should use caution when considering the following kinematic analysis and note that it is intended to represent an idealized model, neglecting error propagation from observations and the Galactic potential. It is likely that any inclusion of errors would detract from the unambiguity of the conclusions drawn here.

6.1. The 2015 data set

Following the mass-dependent trajectories back to the Galactic plane-crossing, the results imply an upper limit for the mass of US 708 of 0.45 $M_\odot$ as any assumed higher mass would result in the trajectory avoiding intersection with the plane altogether. A comparison of inferred current space and ejection velocities with predicted ejection velocity spectra is shown in Fig. 11. Excluding additional momentum being imparted on the ejected runaway through interaction with the supernova ejecta, an assumed mass of 0.3 $M_\odot$ is inconsistent with an terminal WD mass of 1.3 $M_\odot$ (Fig. 11D). Bauer et al. (2019) suggest that ejecta interaction would impart an additional kick of $\sim$180 km s^{-1} on a runaway of 0.344 $M_\odot$. Since this kick would be imparted perpendicular to the donor's orbital motion, the ejection velocity would be increased by $\sim$17 km s^{-1}, still insufficient to allow for consistency. It can therefore be concluded that the mass of US 708 would need to be in the range of $0.27\ M_\odot < M_{US\,708} < 0.29\ M_\odot$ assuming a terminal WD mass of 1.3 $M_\odot$. Assuming a terminal WD mass of 1.4 $M_\odot$, that is, close to the Chandrasekhar mass, it yields a likely range of $0.28\ M_\odot < M_{US\,708} < 0.3\ M_\odot$, consistent

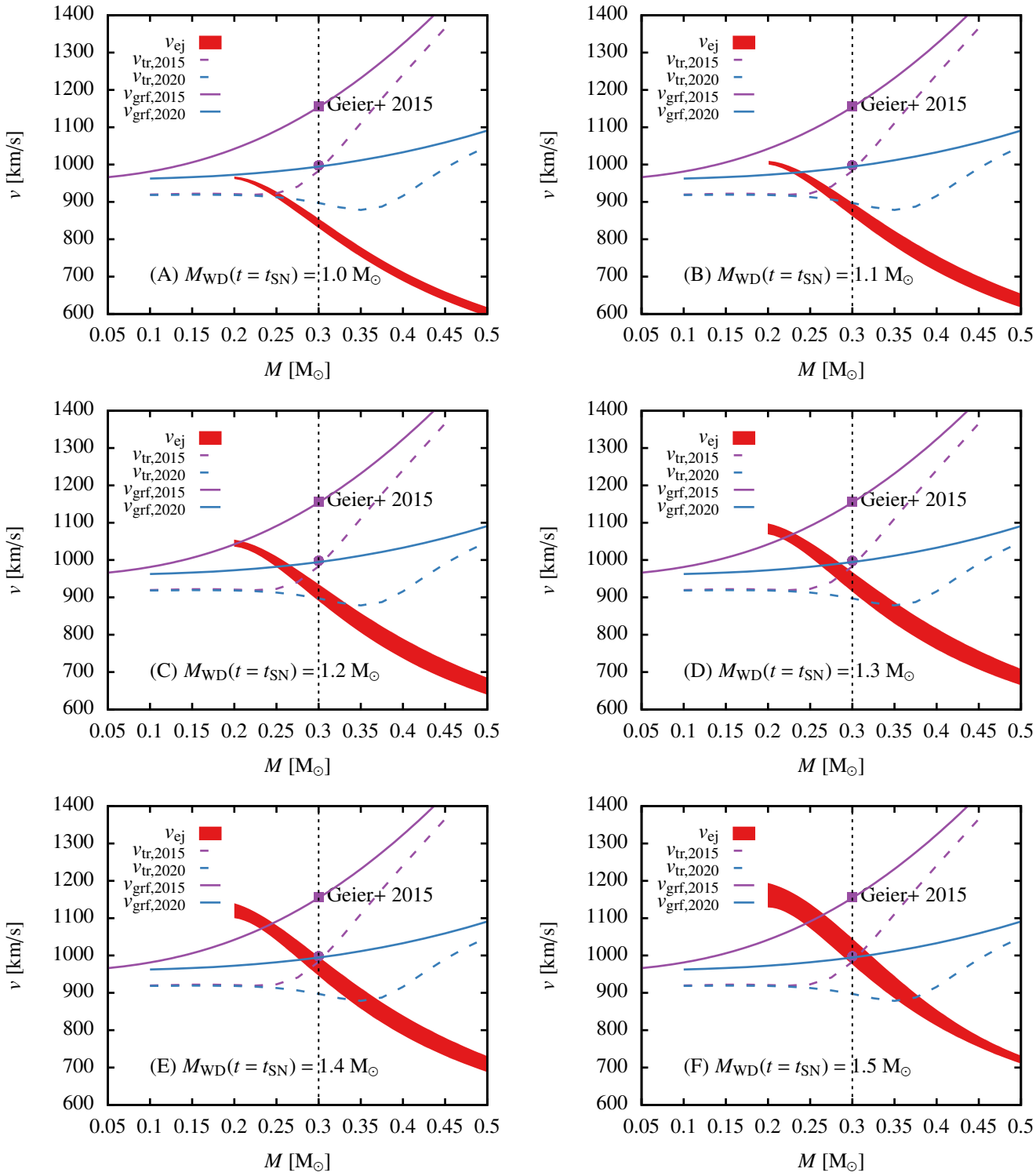

Fig. 11. Inferred current Galactic rest frame velocity, $v_{\rm grf}(t = t_0)$, and ejection velocity, $v_{\rm tr}(t = t_{\rm SN})$, of US 708, as dictated by observed radial velocity and proper motion, correlated with the ejection velocity spectra, $v_{\rm ej}(t = t_{\rm SN})$, with a WD explosion mass ($M_{\rm WD}(t = t_{\rm SN})$) as labeled. Observed space and ejection velocities are base either on Geier et al. (2015) (denoted by subscript "2015") or on proper motions according to *Gaia* DR2 (subscript "2020", Gaia Collaboration 2018) Spectra are represented by the envelopes of their depictions in Fig. 8 for legibility. The current space and inferred ejection velocities, as determined by Geier et al. (2015) are depicted as purple dots.

with the mass adopted by Geier et al. (2015). Assuming a super-Chandrasekhar mass explosion with a terminal WD mass of 1.5 $M_\odot$ would indicate a mass range of 0.29 $M_\odot$ < $M_{\rm US\,708}$ < 0.32 $M_\odot$, also consistent with the mass adopted by Geier et al. (2015). It can be concluded that, if US 708 was ejected in a sub-Chandrasekhar mass SN, then both its terminal and current mass should be smaller than 0.3 $M_\odot$ and it should not currently burn helium. If, on the other hand, US 708 was ejected in a Chandrasekhar or super-Chandrasekhar mass SN, the question of its current state depends on the amount of material stripped

during the SN event, given that it is highly likely that its terminal mass was greater than 0.3 $M_\odot$. It can further be concluded that the observational properties of US 708 in the 2015 data set, including its inferred mass, is most consistent with an origin in a Chandrasekhar or super-Chandrasekhar mass SN. This is in agreement with the conclusions of Geier et al. (2015).

6.2. The 2020 data set

The *Gaia*-based proper motions imply a significantly lower current space velocity of around 994 km s^{-1}, leading to an inferred ejection velocity (again assuming ejection in the Galactic disc) of around 897 km s^{-1} at a location both closer to Earth and the Galactic Center than in the 2015 data set (see Fig. B.2). In this case, the maximum terminal donor mass compatible with eventual crossing of the disc is found to be 0.575 $M_\odot$. Notably, the lower ejection velocity implied by this data set calls into question, assuming a current mass 0.3 $M_\odot$ for US 708, ejection in a Chandrasekhar-mass SN, instead pointing to a terminal accretor mass of between 1.1 $M_\odot$ and 1.2 $M_\odot$ (Figs. 11B and C). This would notably imply an SN involving the DDet mechanism (see Sect. 2.2) and fall somewhere into the parameter space investigated by Nomoto (1982a,b), Woosley & Kasen (2011) and Neunteufel et al. (2017). Assuming ejection in a Chandrasekhar-mass SN, the most likely current mass for US 708 is in the range of $0.34\,M_\odot < M_{\mathrm{US\,708}} < 0.37\,M_\odot$, significantly higher than the assumed mass of 0.3 $M_\odot$. As in the 2015 data set, a great deal depends on the question of whether US 708 is currently burning helium. If its mass is found to be below 0.3 $M_\odot$, then, discounting errors, a Chandrasekhar-mass detonation would be conclusively ruled out. As in the 2015 data set, seen in Fig. 9, a runaway mass greater than 0.4 $M_\odot$ is ruled out for all but significantly super-Chandrasekhar-mass SNe. However, it should be emphasized that the analytical power of correlating ejection velocity spectra and kinematic analysis would be greatly improved if it were carried out with distance measurements that are independent of stellar luminosity and mass estimates, that is, parallax distances.

7. Discussion

Investigations of the runaway velocity of the surviving companions of WDs undergoing thermonuclear SNe are hampered by the unresolved nature of the most likely explosion mechanism. This is usually accompanied by the physics involved in the preceding evolution of the WD undergoing mass accretion being less than certain as well. Less uncertainty is involved in the evolution of the donor star, which can therefore serve as a convenient entry point for the modeling of ejection velocity spectra. Some of the simplifications employed in this study come with a number of caveats. While it was shown here that the initial orbital separation of the progenitor binary has little effect on the expected ejection velocity, previous studies (e.g., Yoon & Langer 2004b; Kato & Hachisu 2004; Neunteufel et al. 2017) suggest that the idiosyncratic evolution of the mass transfer rate associated with certain initial orbital separations do impact the ignition behavior of the accreted material on the WD. Besides calling into question the assumption of conservative mass transfer, as weak helium ignitions may lead to nova-like events, expelling part of the accumulated helium layer from the system, the ability of the accreting WD to accept additional material without triggering a supernova explosion will, in reality, be limited (see e.g. Nomoto 1982a,b; Yoon & Langer 2004b; Neunteufel et al. 2016, 2019). The latter condition can realistically be expected to limit the ejection velocity spectra to those terminal accretor masses compatible with the assumed explosion mechanisms. The impact of non-conservative mass transfer, however, is less straightforward. As mass is lost from the system, compared to the conservative case, the metal content of the donor star will be higher for any combination of donor and accretor mass. As metalicity impacts the radius of the donor star (compare Fig. 2B), the corresponding orbital and, hence, the ejection velocity, can be expected to be lower. The results of these calculations could also be impacted by the effects of tides, especially heating effects, affecting the radius of the donor star, again leading to lower ejection velocities for the same mass combinations (Applegate & Patterson 1987). The results presented here agree well with those of Ergma & Fedorova (1990), and Neunteufel et al. (2016, 2019). However, Wang & Han (2009), using population synthesis to study essentially the same problem, but limiting themselves to $M_{\mathrm{d,f}} > 0.6\,M_\odot$, seem to find less strongly constrained ejection spectra. However, as they do not present ejection velocities in relation to terminal accretor mass, it is difficult to pinpoint the reason for this discrepancy. The most likely reason is the inclusion of bifurcations in the ejection velocity spectra, leading to a larger spread, as seen in Fig. 8A. They further find relatively lower ejection velocities for $M_{\mathrm{d,f}} \sim 0.6\,M_\odot$, as well as higher than previously found possible for $M_{\mathrm{d,f}} \gtrsim 1.0\,M_\odot$ in this study. As their calculations include the evolution of the primordial main sequence binary, a systematic correlation between $M_{\mathrm{d,init}}$ and $M_{\mathrm{WD,init}}$ may be introduced, which is absent from the models in this paper. This may explain the discrepancy at lower $M_{\mathrm{d,f}}$. The discrepancy at higher $M_{\mathrm{d,f}}$ may be explained by differences in metalicity and rotation, both absent from this study. This applicability of the results obtained to observed runaway stars has been discussed at length. With respect to possible progenitor systems, the following objects can be commented upon: Vennes et al. (2012) and Geier et al. (2013), independently showed CD−30°11223 to contain a WD with a mass of 0.75−0.77 $M_\odot$ and a hot subdwarf (sdB) of 0.44−0.48 $M_\odot$ in a detached configuration and a period of $P = 0.04897906 \pm 0.00000004$ d. After entering a semidetached state, the WD in this system would need to accrete a substantial amount of He from its companion in order to become capable of producing an SN.

An object that is of interest in the context of this study is V445 Pup, a nova-like variable that erupted in late 2000. Ashok & Banerjee (2003) argued that this object represents a helium nova event with a WD accretor of 1.35 $M_\odot$ Kato et al. (2008) and a relatively massive 1.2−1.3 $M_\odot$ helium star companion (Woudt et al. 2009). It is currently unknown whether the donor star in this system is a giant or a HeMS star. If the donor can be shown to be a giant, and an SN eventually occurs, then runaway velocities would be too low to produce a HVS. If the donor is a HeMS star, then the fact that it is currently undergoing RLOF indicates that it would have to have filled its Roche lobe immediately after the end of the most recent CE phase. Further considering the mass of the donor, the ejection of a HVS is still unlikely if significant mass cannot be ejected from the system prior to the (assumed) detonation of the accretor. Very recently, the discovery of a very short period binary composed of a $0.337 \pm 0.015\,M_\odot$ helium sdOB and a $0.545 \pm 0.020\,M_\odot$ WD was reported by Kupfer et al. (2020). This system, if it is even capable of producing an SN at all, is unlikely to be able to produce a HVS.

Further theoretical exploration of the parameter space should include explicit treatments of the effects of non-conservative mass transfer and initial metalicity. Variations of the initial orbital separation at low total binary mass should also be

considered. The effects of tidal interaction are likely to prove significant as well.

8. Summary and conclusions

This paper presents a thorough study of the ejection velocity spectra for runaway stars resulting from thermonuclear SNe in the single degenerate helium donor channel.

It has been seen that the structural behavior of the donor star implies the existence of a maximum ejection velocity, which is correlated with the terminal mass of the donor star. The location, albeit not the value, of this maximum, is largely independent of the terminal mass of the accretor, and lies in the range $0.19\,M_\odot < M_\mathrm{d} < 0.25\,M_\odot$. The value of the maximum ejection velocity, on the other hand, is dictated by the terminal mass of the accreting companion, with values correlated with higher terminal masses. It is found that maximum ejection velocities in excess of $1000\,\mathrm{km\,s^{-1}}$ can be attained with terminal accretor masses higher than $1.1\,M_\odot$. This suggests that the SN ejection scenario is able to account for the existence of objects like the hypervelocity runaway sdO US 708 without the need for additional acceleration mechanisms, such as shock interaction. Concurrently, the assumed mass, $M_{\mathrm{US\,708}} = 0.3\,M_\odot$, and inferred ejection velocity of this object in the 2015 data set is most consistent with a Chandrasekhar mass detonation, while more recently obtained proper motions suggest a sub-Chandrasekhar detonation with a terminal mass in the range $1.1\,M_\odot$ to $1.2\,M_\odot$. This result implies that the ejection of US 708 is compatible with its progenitor being identified as a single degenerate, helium accreting WD undergoing an SN, according to the double detonation mechanism as proposed by Nomoto (1982a,b). Assuming a Chandrasekhar mass detonation with the 2020 data set would imply that the current mass of US 708 lies in the range $0.34\,M_\odot < M_{\mathrm{US\,708}} < 0.37\,M_\odot$.

The maximum itself is a result of the mass transfer rate in the system exceeding the critical rate allowing for a decrease in orbital separation due to emission of GWR and transfer of orbital angular momentum due to mass transfer. Since the maxima of the ejection velocity spectra are associated with terminal donor star masses below $0.3\,M_\odot$, that is, below the limit required for a star to retain the ability to burn helium, ejection at the highest velocities suggests that these objects are structurally different from slower ones and may result in the eventual production of single hypervelocity ELM WDs. This would be significant as ELM occurrence is currently thought to be dominated by binaries. The production of a runaway with a mass higher than $0.3\,M_\odot$ and exceeding $1000\,\mathrm{km\,s^{-1}}$ requires a terminal accretor mass in excess of the Chandrasekhar mass. Therefore, observation of a hypervelocity hot subdwarf with $v_\mathrm{ej} > 1000\,\mathrm{km\,s^{-1}}$ in its core helium-burning phase would conclusively rule out sub-Chandrasekhar mass ejection in the SN scenario for that star. In the same vein, the observation of objects moving faster than the ejection velocity maximum would conclusively rule out SD SN ejection with the respective accretor mass.

While practicable studies of HVS ejection velocities for the purposes of the investigation of SD SN explosion mechanisms will require both more accurate observations and larger sample sizes than currently available, as demonstrated, they have the potential to provide constraints on terminal SN progenitor states that are not accessible to current observational techniques. In the future, data provided by large scale astrometry experiments such as *Gaia* (Gaia Collaboration 2018) and the upcoming 4MOST instrument (de Jong et al. 2016) may be able to provide a sufficient number of observations.

Acknowledgements. Assistance of the Science and Technologies Facilities Council (UK), grant No. ST/S000453/1, is gratefully acknowledged. The author would like to thank Sergei Nayakshin, Phillip Podsiadlowski, Stephen Justham and Stephan Geier for useful discussions and Ulrich Heber for constructive suggestions which helped improve the paper.

References

Abadi, M. G., Navarro, J. F., & Steinmetz, M. 2009, ApJ, 691, L63
Allen, C., & Santillan, A. 1991, Rev. Mex. Astron. Astrofis., 22, 255
Applegate, J. H., & Patterson, J. 1987, ApJ, 322, L99
Arnett, W. D. 1969, Ap&SS, 5, 180
Arnett, W. D. 1971, ApJ, 169, 113
Ashok, N. M., & Banerjee, D. P. K. 2003, A&A, 409, 1007
Bauer, E. B., White, C. J., & Bildsten, L. 2019, ApJ, 887, 68
Blaauw, A. 1961, Bull. Astron. Inst. Neth., 15, 265
Bromley, B. C., Kenyon, S. J., Geller, M. J., et al. 2006, ApJ, 653, 1194
Brooks, J., Schwab, J., Bildsten, L., Quataert, E., & Paxton, B. 2017, ApJ, 843, 151
Brown, W. R. 2015, ARA&A, 53, 15
Brown, W. R., Geller, M. J., Kenyon, S. J., & Kurtz, M. J. 2005, ApJ, 622, L33
Brown, W. R., Geller, M. J., Kenyon, S. J., Kurtz, M. J., & Bromley, B. C. 2007, ApJ, 671, 1708
Brown, W. R., Kilic, M., Kosakowski, A., et al. 2020, ApJ, 889, 49
de Jong, R. S., Barden, S. C., Bellido-Tirado, O., et al. 2016, in Ground-based and Airborne Instrumentation for Astronomy VI, Proc. SPIE, 9908, 99081O
de la Fuente Marcos, R., & de la Fuente Marcos, C. 2019, A&A, 627, A104
Di Stefano, R., Voss, R., & Claeys, J. S. W. 2011, ApJ, 738, L1
Edelmann, H., Napiwotzki, R., Heber, U., Christlieb, N., & Reimers, D. 2005, ApJ, 634, L181
Eggleton, P. P. 1983, ApJ, 268, 368
Eggleton, P. 2011, Evolutionary Processes in Binary and Multiple Stars (Cambridge: Cambridge University Press)
Ergma, E. V., & Fedorova, A. V. 1990, Ap&SS, 163, 143
Erkal, D., Boubert, D., Gualandris, A., Evans, N. W., & Antonini, F. 2019, MNRAS, 483, 2007
Fink, M., Hillebrandt, W., & Röpke, F. K. 2007, A&A, 476, 1133
Gaia Collaboration (Brown, A. G. A., et al.) 2018, A&A, 616, A1
Gamezo, V. N., Khokhlov, A. M., & Oran, E. S. 2005, ApJ, 623, 337
Geier, S., Marsh, T. R., Wang, B., et al. 2013, A&A, 554, A54
Geier, S., Fürst, F., Ziegerer, E., et al. 2015, Science, 347, 1126
Hachisu, I., Kato, M., Saio, H., & Nomoto, K. 2012, ApJ, 744, 69
Han, Z. 2008, ApJ, 677, L109
Hansen, C. J., & Wheeler, J. C. 1969, Ap&SS, 3, 464
Heber, U. 2009, ARA&A, 47, 211
Heber, U. 2016, PASP, 128, 082001
Hillebrandt, W., & Niemeyer, J. C. 2000, ARA&A, 38, 191
Hills, J. G. 1991, AJ, 102, 704
Hills, J. G. 1992, AJ, 103, 1955
Hills, J. G. 1988, Nature, 331, 687
Hirsch, H. A., Heber, U., O'Toole, S. J., & Bresolin, F. 2005, A&A, 444, L61
Hoogerwerf, R., de Bruijne, J. H. J., & de Zeeuw, P. T. 2001, A&A, 365, 49
Howell, D. A., Sullivan, M., Nugent, P. E., et al. 2006, Nature, 443, 308
Hoyle, F., & Fowler, W. A. 1960, ApJ, 132, 565
Hut, P. 1981, A&A, 99, 126
Irrgang, A., Wilcox, B., Tucker, E., & Schiefelbein, L. 2013, A&A, 549, A137
Irrgang, A., Kreuzer, S., & Heber, U. 2018, A&A, 620, A48
Irrgang, A., Geier, S., Heber, U., Kupfer, T., & Fürst, F. 2019, A&A, 628, L5
Justham, S., Wolf, C., Podsiadlowski, P., & Han, Z. 2009, A&A, 493, 1081
Kato, M., & Hachisu, I. 2004, ApJ, 613, L129
Kato, M., Hachisu, I., & Kiyota, S. 2008, in Hydrogen-Deficient Stars, eds. A. Werner, & T. Rauch, ASP Conf. Ser., 391, 267
Khokhlov, A. M., Oran, E. S., & Wheeler, J. C. 1997, ApJ, 478, 678
Kippenhahn, R., Weigert, A., & Weiss, A. 2012, Stellar Structure and Evolution (Berlin, Heidelberg: Springer-Verlag)
Koposov, S. E., Boubert, D., Li, T. S., et al. 2020, MNRAS, 491, 2465
Kupfer, T., Bauer, E. B., Marsh, T. R., et al. 2020, ApJ, 891, 45
Landau, L., & Livshitz, E. 1975, The Classical Theory of Fields, Course of Theoretical Physics (Oxford: Butterworth Heinemann)
Liu, W. M., Chen, W. C., Wang, B., & Han, Z. W. 2010, A&A, 523, A3
Livne, E., & Arnett, D. 1995, ApJ, 452, 62
Mestel, L. 1968, MNRAS, 138, 359
Neunteufel, P., Yoon, S.-C., & Langer, N. 2016, A&A, 589, A43
Neunteufel, P., Yoon, S.-C., & Langer, N. 2017, A&A, 602, A55
Neunteufel, P., Yoon, S. C., & Langer, N. 2019, A&A, 627, A14
Nomoto, K. 1980, in Texas Workshop on Type I Supernovae, ed. J. C. Wheeler, 164

Nomoto, K. 1982a, ApJ, 257, 780
Nomoto, K. 1982b, ApJ, 253, 798
Nomoto, K., Thielemann, F. K., & Yokoi, K. 1984, ApJ, 286, 644
O'Leary, R. M., & Loeb, A. 2008, MNRAS, 383, 86
Pakmor, R., Kromer, M., Taubenberger, S., & Springel, V. 2013, ApJ, 770, L8
Paxton, B., Bildsten, L., Dotter, A., et al. 2011, ApJS, 192, 3
Paxton, B., Cantiello, M., Arras, P., et al. 2013, ApJS, 208, 4
Paxton, B., Marchant, P., Schwab, J., et al. 2015, ApJS, 220, 15
Paxton, B., Schwab, J., Bauer, E. B., et al. 2018, ApJS, 234, 34
Paxton, B., Smolec, R., Schwab, J., et al. 2019, ApJS, 243, 10
Phillips, M. M. 1993, ApJ, 413, L105
Piffl, T., Scannapieco, C., Binney, J., et al. 2014, A&A, 562, A91
Plewa, T., Calder, A. C., & Lamb, D. Q. 2004, ApJ, 612, L37
Press, W. H., Teukolsky, S. A., Vetterling, W. T., & Flannery, B. P. 1992, Numerical Rrecipes in C. The Art of Scientific Computing (Cambridge: Cambridge University Press)
Raddi, R., Hollands, M. A., Koester, D., et al. 2019, MNRAS, 489, 1489
Ritter, H. 1988, A&A, 202, 93
Scholz, R.-D. 2018, Res. Notes Am. Astron. Soc., 2, 211
Sesana, A., Madau, P., & Haardt, F. 2009, MNRAS, 392, L31
Shen, K. J., Boubert, D., Gänsicke, B. T., et al. 2018, ApJ, 865, 15
Sim, S. A., Röpke, F. K., Hillebrandt, W., et al. 2010, ApJ, 714, L52
Soker, N. 2013, in Binary Paths to Type Ia Supernovae Explosions, eds. R. Di Stefano, M. Orio, & M. Moe, IAU Symp., 281, 72
Tauris, T. M. 2015, MNRAS, 448, L6
Tutukov, A. V., & Yungelson, L. R. 1979, Acta Astron., 29, 665
Vennes, S., Kawka, A., O'Toole, S. J., Németh, P., & Burton, D. 2012, ApJ, 759, L25
Vennes, S., Nemeth, P., Kawka, A., et al. 2017, Science, 357, 680
Wang, B., & Han, Z. 2009, A&A, 508, L27
Wang, B., Justham, S., & Han, Z. 2013, A&A, 559, A94
Webbink, R. F. 1984, ApJ, 277, 355
Woosley, S. E., & Kasen, D. 2011, ApJ, 734, 38
Woosley, S. E., & Weaver, T. A. 1994, ApJ, 423, 371
Woudt, P. A., Steeghs, D., Karovska, M., et al. 2009, ApJ, 706, 738
Yoon, S.-C., & Langer, N. 2004a, A&A, 419, 645
Yoon, S.-C., & Langer, N. 2004b, A&A, 419, 623
Yoon, S.-C., & Langer, N. 2005, A&A, 435, 967
Yu, Q., & Tremaine, S. 2003, ApJ, 599, 1129
Yungelson, L. R. 2008, Astron. Lett., 34, 620
Zhang, M., Fuller, J., Schwab, J., & Foley, R. J. 2019, ApJ, 872, 29

Appendix A: Effects of initial orbital separation

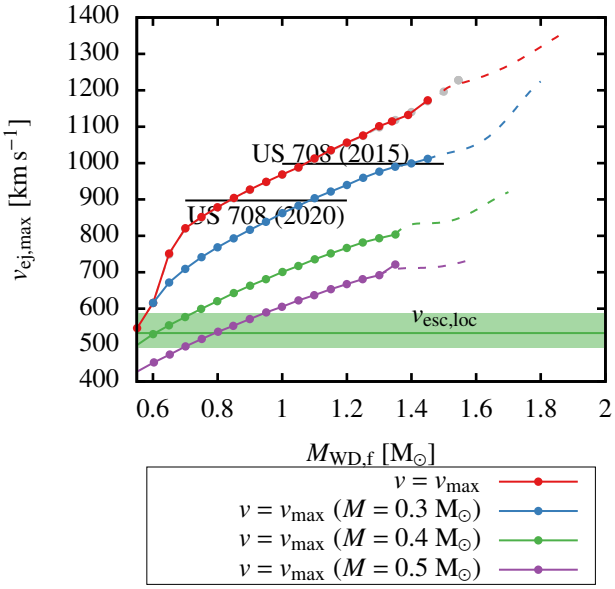

Fig. A.1. As in Fig. 9, but $a_{init}(\xi = 1.01)$ (see Sect. 4). The gray line indicates v_{max} as in Fig. 9 for comparison.

As described in Sect. 4, the initial orbital separations $a_{init}(\xi)$ used in this paper were chosen such that Eq. (1) satisfies $R_{d,RL} = \xi \cdot R_d$ with $\xi = 1.005$. Since this choice results in a varied range of initial orbital separations and initial periods, the orbital separations and initial periods will not be comparable between individual systems, even between systems with equal total or component masses. As argued, the window for RLOF during the HeMS of the donor star is quite narrow in terms of ξ and the effect of a different choice of that parameter on the expected ejection velocity correspondingly small. In order to test this argument, the full grid was rerun with initial orbital separations corresponding to $\xi = 1.01$.

As seen in Fig. A.1, the maximum ejection velocity with $\xi = 1.01$ is not significantly increased compared with $\xi = 1.005$ at the same mass with analogous $M_{d,f}$. It can reasonably concluded that the initial orbital separation is of secondary importance for the question of ejection velocity maxima. However, due to the desire to access the entire mass spectrum with two sets of initial models, this increase is small. While the predictive power hat high values of $M_{d,init}$ can be called reasonable, more work is required in cases of low $M_{d,init}$.

Appendix B: HVS kinematic analysis

Trajectory and time-of-flight data as described in Sect. 6 were calculated by numerically solving the Newtonian equations of motion in the well known form,

$$m\frac{d}{dt}\frac{dx}{dt} = -\nabla\Phi(x), \tag{B.1}$$

with Φ the Galactic potential. The numerical solver utilized here was newly developed on the basis of a fourth-order Runge-Kutta integrator with adaptive step size control as described by Press et al. (1992). The Galactic potential was assumed to be static and correspond to Model 1 put forward by Irrgang et al. (2013) as a revision of Allen & Santillan (1991) in the form,

Table B.1. Parameters used in Eqs. (B.2)–(B.4).

	$M_{b/d/h}$ [M_G]	$a_{d/h}$ [kpc]	$b_{b/d/h}$ [kpc]	Λ [kpc]
Bulge$_b$	409 ± 63		0.23 ± 0.03	
Disk$_d$	2856^{+376}_{-202}	$4.22^{+0.53}_{-0.99}$	$0.292^{+0.020}_{-0.025}$	
Halo$_h$	1018^{+27933}_{-603}	$2.562^{+25.963}_{-1.419}$	$4.22^{+0.53}_{-0.99}$	200^{+0}_{-82}

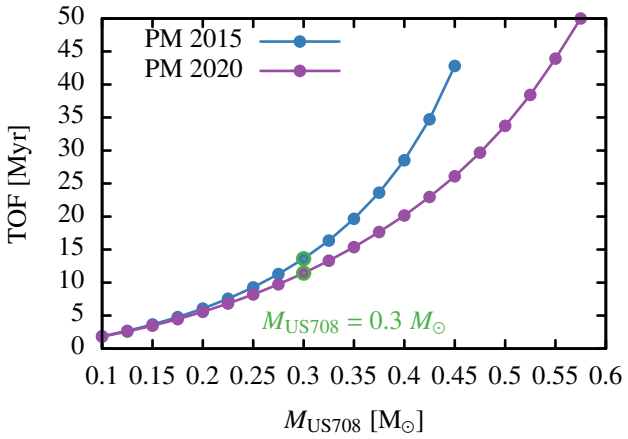

Fig. B.1. Mass-dependent time of flight (TOF) since ejection from the disc for US 708, once for proper motions as obtained by Geier et al. (2015) and once for proper motions as published by *Gaia* DR2 (Gaia Collaboration 2018). The preferred model with $M_{US\,708} = 0.3\,M_\odot$ is highlighted in green. Note that the counter-intuitively shorter TOF at similar mass obtained for the slower space velocity of the 2020 data set is a result of the shorter distance traveled to the disc-crossing point. This shorter distance, in turn, is derived from the reoriented direction of travel as compared to the 2015 data set (see Fig. B.2).

$$\Phi_b(R) = -\frac{M_b}{\sqrt{R^2 + b_b^2}}, \tag{B.2}$$

for the bulge, where R is the distance from the Galactic Center,

$$\Phi_d(r,z) = -\frac{M_d}{\sqrt{r^2 + (a_d + \sqrt{z^2 + b_d^2})}}, \tag{B.3}$$

for the disk, where r is the distance from the Galactic Center in the x–y-plane and z is the distance from the x–y-plane and

$$\Phi_h(R) = -\frac{M_h}{a_h}\left[\frac{1}{\gamma - 1}\ln\left(\frac{1 + (R/a_h)^{\gamma-1}}{1 + (\Lambda/a_h)^{\gamma-1}}\right) - \frac{(\Lambda/a_h)^{\gamma-1}}{(1 + \Lambda/a_h)^{\gamma-1}}\right] \text{ if } R < \Lambda$$
$$= -\frac{M_h}{R}\frac{(\Lambda/a_h)^{\gamma-1}}{(1 + \Lambda/a_h)^{\gamma-1}} \text{ if } R \geq \Lambda, \tag{B.4}$$

with $\gamma = 2$ and the other parameters given in Table B.1.

The distance of the Sun from the Galactic Center is given as $r_{Sol} = 8.40 \pm 0.08$ kpc. Using the trajectory solver with the parameters as described above and allowing the inferred mass of US 708 to serve as a free parameter, as described in Sect. 6, the time-of-flight (Fig. B.1) and ejection location (Fig. B.2) can be calculated. Results for both time-of-flight and ejection location are in good agreement with the more detailed calculations presented by Geier et al. (2015) for the preferred model of $M_{US\,708} = 0.3\,M_\odot$.

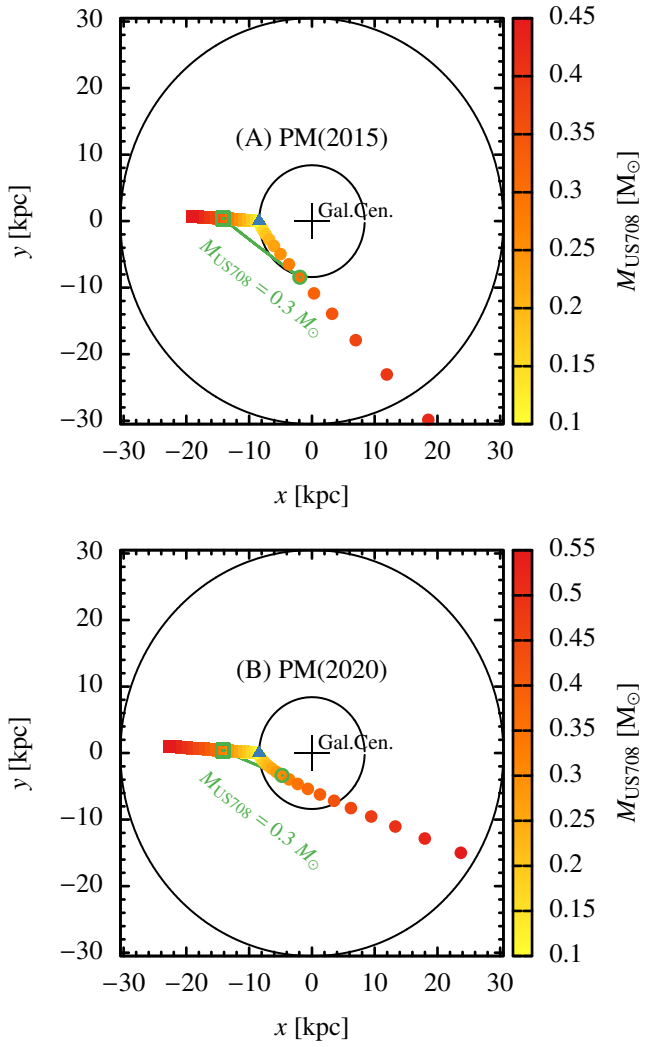

Fig. B.2. Current inferred location, depending on assumed mass ($M_{\mathrm{US\,708}}$) of US 708, and inferred origins relative to the Galactic center and the position of the Sun in the Galactic x–y plane. *Panel A*: proper motions as obtained by Geier et al. (2015), *panel B*: proper motions obtained by *Gaia* (Gaia Collaboration 2018). The location, origin and past trajectory of the preferred model with $M_{\mathrm{US\,708}} = 0.3\,M_\odot$ is highlighted in green.